Zinc Ion Thermogalvanic Cell: A New Strategy for Low-Grade Heat Conversion and Energy Storage

Zhiwei Li
Nanjing University of Aeronautics and Astronautics https://orcid.org/0000-0003-2526-1744
Yinghong Xu
Nanjing University of Aeronautics and Astronautics
Langyuan Wu
Nanjing University of Aeronautics and Astronautics
Yufeng An
Nanjing University of Aeronautics and Astronautics
Yao Sun
Nanjing University of Aeronautics and Astronautics
Tingting Meng
Nanjing University of Aeronautics and Astronautics
Hui Dou
Nanjing University of Aeronautics and Astronautics
Yimin Xuan
Nanjing University of Aeronautics and Astronautics
Xiaogang Zhang (azhangxg@nuaa.edu.cn)
Nanjing University of Aeronautics and Astronautics https://orcid.org/0000-0003-0484-2451

Article

Keywords: batteries, energy storage, low-grade heat

Posted Date: July 20th, 2021

DOI: https://doi.org/10.21203/rs.3.rs-702045/v1

Version of Record: A version of this preprint was published at Nature Communications on January 10th, 2022. See the published version at https://doi.org/10.1038/s41467-021-27755-x.

Abstract

Converting low-grade heat from environment into electricity shows great sustainability for mitigating the energy crisis and adjusting energy configuration. However, the thermally rechargeable devices suffer from poor Seebeck coefficient when a semiconductor or ionic electrolyte is typically employed. Breaking the convention of thermoelectric systems, we propose and demonstrate a new zinc ion thermogalvanic cell to generate electricity from low-grade heat via the thermo-extraction/insertion and thermodiffusion process of insertion-type cathode (VO_2-PC) and stripping/plating behavior of Zn anode. Based on this strategy, a high thermopower of ~ 15 mV k^{-1} and an excellent output power of 1.2 mW can be impressively obtained. Besides, a high specific capacity and a superior durability are originated from coupling of VO_2-PC and Zn. This work with extraordinary energy conversion efficiency and satisfying energy storage capability will pave the way toward construction of thermoelectric setups with attractive property for high value-added utilization of low-grade heat.

Introduction

High value-added utilization of plentiful but also sustainable heat power has spurred urgent development of cost-effective and safe technologies for harvesting low-grade heat (< 100 ºC) into electricity.[1–3] Among various advanced systems, the electronic thermoelectric device (e-TE) using narrow-bandgap semiconductors can realize the conversion of low-grade heat to fulfill the requirements of electronic markets based on the Seebeck effect. Typically, as-obtained Seebeck coefficient (α) for the e-TE is only ~ 100 μV K^{-1}.[4] As a result, it is very challenging to generate a satisfying voltage from 1 to 5 V by the integration of numerous e-TEs. Therefore, a new-type thermogalvanic cell with enhanced performance has to be further designed and considered.

Recently, an alternative approach named ionic thermoelectric device (i-TE) was adopted to the direct energy harvesting, which delivers two different mechanisms including thermogalvanic effect and thermodiffusion effect.[2,5] Low-grade heat can be continuously converted into electricity because a temperature difference can induce a voltage difference. For instance, a thermally chargeable supercapacitor was demonstrated by Zhang and co-workers based on the thermodiffusion effect. An α value of 1.21 mV K^{-1} can be obtained at a temperature difference of 52 K with 1.0 mol L^{-1} KNO_3 electrolyte.[6] To improve the temperature coefficient, a lot of researches employed aqueous electrolytes with the addition of redox couples like ferro/ferricyanide [$Fe(CN)_6^{4-}$/$Fe(CN)_6^{3-}$].[2,5,7–10] Liu et al has reported an ionic thermoelectric materials using KCl and [$Fe(CN)_6^{4-}$/$Fe(CN)_6^{3-}$] for the synergistic effect of thermogalvanic and thermodiffusion.[2] Consequently, a superior α value of 17.0 mV K^{-1} was achieved using body heat and an output voltage over 2 V was generated by integrating 25 unipolar units. Although great efforts for e-TEs and i-TEs have been contributed to realize high-efficient conversion of low-grade heat, the output voltage is highly limited by their symmetric feature and the energy storage mechanism near electrode/electrolyte interface. It is reasonable to propose that the construction of hybrid device

based on the Soret effect may exhibit huge potential in the harvesting of electricity under steady temperature gradient.

To a literature survey, aqueous zinc ion batteries (ZIBs) have been emerging as a promising candidate for energy storage due to the merits of Zn anode, including its cost-effectiveness, multivalent feature and satisfactory stability.[11–13] To achieve an optimized performance of ZIBs, various cathode materials such as manganese-based oxides, transition metal-based compounds, Prussian blue analogs, and organic materials have been developed. When introducing the concept of ZIBs into heat-to-electricity conversion, various mechanisms can be proposed through the synergistic effect between thermodiffusion and thermoextraction effects (Fig. 1). The Zn-based thermally chargeable supercapacitors (ZTSCs) using capacitive cathodes (*i.e.* PC) could generate electricity based on the thermodiffusion effect along with the stripping and plating of Zn anode. Typically, the applied temperature gradients can cause both cations and anions to migrate from the hot side to cold side (Fig. 1a). A thermodiffusive voltage can be generated and defined as $\Delta V_{td} = -(\hat{u}_H - \hat{u}_C)/e$. As known, the intercalated Zn^{2+} migrate to the surface of Zn anode and spontaneous experience a stripping process. Based on the extraction of ions inserted in the selected cathode, the transferred charges to the hot side reasonably improves the obtained electrochemical potential (Fig. 1b). However, the relatively sluggish kinetics of pure battery-like systems greatly limits the practical applications. Reasonably, the Zn-based thermogalvanic cells (ZTGCs), which combine the thermodiffusion of ions on PC and the extraction of ions from insertion-type cathodes can output a higher voltage (Fig. 1c). As known, vanadium-based oxides demonstrate promising performances owing to their high multiple valence feature and unique crystal structure for ions storage.[11,13,14] However, the sluggish kinetics, poor conductivity and structure deterioration involved in the insertion/extraction of Zn^{2+} always impede their large-scale applications, that is, the rational design of satisfying vanadium-based oxides to fulfill the requirements of energy storage and conversion is still in its infancy.

Herein, we developed a promising ZTGCs by the combination of electroactive VO_2 and conductive porous carbon (VO_2-PC) with a universal metal coordination. Such compositions not only provide more electrochemical sites and channels for electrolyte ions, but also enhance the diffusion kinetics of ions. As a result, the VO_2-PC shows promising capacity, good rate capability and excellent durability. Moreover, the proposed VO_2-PC based ZTGC can generate electricity from low-grade heat through the synergistic effect of thermodiffusion and thermoextration behaviors. Furthermore, the proof-of-concept setup displays satisfying application potential in harvesting energy from waste heat due to its ultrahigh output voltage of ~ 1 V with only one unit.

Results

Preparation and characterization of VO_2-PC nanosphere. The spherical vanadium-polydopamine (V-PDA) composites were rationally synthesized by a unique metal coordination strategy between dopamine and ammonium metavanadate. After pyrolysis under nitrogen atmosphere, the PDA and V-based species were evolved into hierarchical porous carbon (PC) matrix and anchored vanadium dioxide (VO_2) along

with gas escape, and the details can be seen in the Experimental section. Field-emission scanning electron microscope (FESEM) and transmission electron microscope (TEM) were employed to observe the microstructures of as-prepared materials. It can be found that the morphology of pure PDA derived PC is uneven nanospheres with different diameters ranging from 100 nm to ~ 1 μm (Fig. S1). In particular, the VO_2-PC is engineered by uniform nanospheres with a size of about 250 nm (Fig. 1a and b). Because the catechol groups of dopamine can strongly coordinate with divalent metal ions, the metal ions can be effectively adsorbed.[15] Thus, the VO_2 is uniformly distributed in the VO_2-PC sample with a high content of 65.4 wt% determined by the thermogravimetric analyses owing to the fine molecular-level coordination between active metal centers and organic molecule (Fig. S2). Through the obvious spherical morphology (Fig. 1c), it is can be noted that the porous VO_2-PC shows amorphous feature. From the HRTEM image of VO_2-PC (inset of Fig. 1c), a lattice fringe with the spacing of 0.353 nm can be attributed to the (110) plane of monoclinic VO_2. Such unique integration of VO_2 and porous carbon in the VO_2-PC would be beneficial to provide abundant pathways and electroactive sites for Zn^{2+} diffusion and storage, which could enhance the rate capability and specific capacity of as-designed devices. The energy dispersive X-ray spectrometry (EDX) elements mapping images in Fig. 1d further confirm the coexistence and extremely even distribution of C, N, O, and V elements in the VO_2-PC sphere. The X-ray diffraction (XRD) pattern of VO_2-PC is displayed in Fig. 1e, in which almost all the peaks can be well indexed to monoclinic VO_2 (PDF#81-2392).[16] The crystal structure of layered VO_2 is presented in the inset of Fig. 1e, and relatively large one-dimensional tunnels are formed by the shared corners of V_4O_{10} in VO_2, implying fast transport of electrolyte ions. There are six main peaks existed in the Raman spectrum of VO_2-PC (Fig. 1f), which can be corresponded to the layered structure of VO_2 crystalline (140.2 cm^{-1}), V = O bending vibration (279.4 and 406.7 cm^{-1}), V-O-V stretching vibration (686.9 cm^{-1}), and V = O stretching vibration (992.6 cm^{-1}).[17] Besides, the valence of V element was investigated by the X-ray photoelectron spectroscopy (XPS) spectrum in Fig. 1f. As analyzed, only V^{4+} exists in the obtained product, which suggests the successful preparation of standard VO_2.[18] More importantly, when using molybdenum (Mo) and tungsten (W) as the metal sources, this proposed strategy also can reasonably form the corresponded Mo_4O_8-PC and W_3O_9-PC, as proved by the SEM images and XRD results (Fig. S3).

Electrochemical performance of ZTGCs. To accurately evaluate the practical application of electrode materials in the conversion of low-grade heat, we have constructed a non-isothermal H cell with Zn-G anode and VO_2-PC cathode, as illustrated in Fig. 3a. During the measurements, the VO_2-PC cathode is heated by hot water bath while the Zn-G anode is unheated to form a temperature difference (ΔT). It should be noted that the ΔT between anode and cathode is detected by the thermocouple inserted in each chamber. To minimize the kinetics effects, an ultralow current of 40 μA was applied to various electrodes without temperature gradient (Fig. 3b). Clearly, the VO_2-PC combines the characteristics of both PC and VO_2, which endows VO_2-PC electrode with a shorter time to achieve the open circuit voltage than pure VO_2 under this case. The fast increase of voltage at initial state is mainly caused by the desorption of electrolyte ions. Meanwhile, the weaken platforms appeared in both VO_2 and VO_2-PC are assigned to the

extraction of ions. The evolution of the output voltage (ΔV) under various temperature differences for the VO_2-PC, VO_2 and PC based ZTGCs are profiled in Fig. 3c. As we gradually increase the heat input, the temperature difference and output voltage can achieve a series of steady states within 2400 s. Notably, the output voltage is dramatically increased with a ΔT of 5 K for PC based ZTGC, which mainly caused by the fast desorption of electrolyte ions. When the ΔT reaches 10 K, a relatively stable voltage of ~ 1.1 V can be obtained. Interestingly, the voltage endowed by such ion desorption is relatively weakened and only ~ 0.5 V can be achieved for VO_2-PC, which is also higher than that of VO_2 (~ 0.4 V). This significant difference between PC and VO_2-PC may be highly influenced by their different charge storage mechanisms. As discussed above, the inserted Zn^{2+} can react with the VO_2 and achieve stable bonding in the form of chemical bonds.[19] Thus, a large plenty of heat is required to release such combined Zn^{2+}, which also implies a high energy input. Consequently, a comparable output voltage of ~ 1.01 V can be delivered from the VO_2-PC based ZTGC under the temperature difference of 45 K. However, only ~ 0.87 V is achieved for VO_2-PC based setup due to the sluggish extraction of ions from the highly ordered crystals. Figure 3d summarizes the detailed output voltage value at various temperature differences of as-constructed ZTGCs. Obviously, the increasing trend of ΔV is highly consistent with the kinetics of adsorption/desorption and insertion/extraction. According to the relationship between ΔV and ΔT, the temperature/Seebeck coefficient (α) can be calculated, which is described by the following equation:[6,20]

$$\alpha = \frac{\Delta V}{\Delta T} \quad (1)$$

As shown in Fig. 3e, the Seebeck coefficient is rapidly decreased during the fast desorption of electrolyte ions (stage I). As the increase of ΔT, the α value is gradually increased with the extraction of inserted ions. It is worth mentioning that a temperature coefficient as high as 15 mV k^{-1} can be hold under the ΔT of 35 K in stage II. Moreover, the α value is slightly decreased to 14.7 mV k^{-1} at 40 K in stage III, which implies that the extraction of such combined ions with VO_2 crystals needs more heat input. Compared with the pure VO_2, the lower α value of VO_2-PC at stage II is due to the partly expose of embedded VO_2 crystal in carbon matrix and the higher value at stage III is probably caused by its amorphous feature. For convenience, the optimized crystal structures of VO_2, Zn-VO_2, and Zn/H_2O-VO_2 are displayed in Fig. 3f. The possible electrochemical processes involved in both electrodes can be described as follows:

Cathode:

$$VO_2 + xZn^{2+} + yH_2O + 2xe^- \leftrightarrow Zn_xVO_2 \cdot yH_2O \quad (2)$$

Anode:

$$xZn \leftrightarrow xZn^{2+} + 2xe^- \quad (3)$$

With the change of ΔT, the reversible "breathing" of VO_2 unit cell together with the insertion/extraction of electrolyte ions can realize the continuous conversion and utilization of low-grade heat by the synergistic effect. Motivated by the high voltage of as-assembled ZTGCs, a fixed resistor (17 kΩ) was employed to study the corresponded rechargeable behavior. Significantly, the energy decay and thermocharging behavior of VO_2-PC based ZTGC is much comparable than that of PC and VO_2 based ZTGC even over 3000 s (15 cycles) with a stable voltage of 0.9 V, demonstrating the satisfying performance of VO_2-PC based ZTGC in electronics (Fig. 3g). It is worth mentioning that the relatively rapid chargeability of ZTGCs within 100 s can be highly determined by their low energy decay and fast charge response. Furthermore, a series of fixed resistor were used to investigate the power density (P) according to $P = V^2/R$. More excitingly, an ultrahigh power density of 10.8 W m^{-2} can be fitted by VO_2-PC based ZTGC with a load resistor of 200 ~ 470 Ω, which is much better than that of PC and VO_2 based ZTGCs (Fig. 3h). When comparing the output voltage and power of ZTGCs with other reported systems, such as-built devices are hundreds of times that of some ionic thermoelectric devices and three orders of magnitude higher than previously reported electronic-thermoelectric devices (Fig. 3i), demonstrating the availability of ZTGCs as promising devices for low-grade heat conversion.[2,8,21–24]

Energy storage behavior of ZIBs. To evaluate the energy storage ability of as-constructed devices, the ZIBs are reasonably carried out. Figure 4a profiles the cyclic voltammetry (CV) curves of VO_2-PC-based ZIB at a scan rate of 0.2 mV s^{-1}. Clearly, two pairs of redox peaks at around 0.56/0.68 V and 0.92/1.01 V can be corresponded to the multiple insertion/extraction procedures of electrolyte ions in VO_2.[25] The almost overlapping CV curves at initial three cycles further indicate the highly reversible electrochemical behaviors. Besides, the VO_2-PC displays the largest enclosed CV area among PC and commercial VO_2, suggesting its highest charge storage ability (Fig. S4a). The galvanostatic charge/discharge (GCD) curves at a low current density of 0.2 A g^{-1} are in keeping with the same redox reactions of CV curves (Fig. 4b). As a result, a high discharge capacity of 539 mAh g^{-1} can be achieved for the VO_2-PC at this case, which is significantly higher than that of the VO_2 (303.8 mAh g^{-1}) and the PC (49.3 mAh g^{-1}). Meanwhile, the highly reversible behavior and rate capability of VO_2-PC are investigated by GCD tests at various current densities from 0.1 to 20 A g^{-1} (Fig. S4b). Compared to the VO_2 and PC, the VO_2-PC exhibits an excellent capacitive performance together with high reversibility at each rate (Fig. 4c). Impressively, the reversible discharging capacity can still retain 80 mAh g^{-1} even at a high rate of 20 A g^{-1}. When the current density was adjusted back to 0.1 A g^{-1}, the specific capacity can be nearly recovered to 530 mAh g^{-1}, which maintains about 91% of the initial discharging capacity. The corresponding GCD curves of the VO_2-PC based ZIB at different current densities are plotted in Fig. S4c. The obvious electrochemical platforms appeared in the charging and discharging curves directly confirm the mixed energy storage processes endowed by V-species. Ragone plots show the satisfying rate capability of VO_2-PC. As summarized in Fig. S4d, both a superior energy density of 442 Wh kg^{-1} at 112 W kg^{-1} and a high power density of 14.8 kW kg^{-1} at 43 Wh kg^{-1} can be reached based on the cathode mass, which surpasses those of the other devices with PC and VO_2 as electrode materials. Most importantly, the

specific capacity of VO_2-PC based ZIB still can retain approximately 100 mAh g^{-1} even over 50000 cycles at a relatively high current density of 10 A g^{-1}, and the corresponding Coulombic efficiency is about 100% for each cycle (Fig. 4d). Such results also are dramatically higher than that of PC and VO_2 based ZIBs (Fig. S4e). Compared with the previously reported vanadium-based cathodes for aqueous ZIBs, the VO_2-PC electrode displays outstanding performances in terms of specific capacity, cyclic stability, and energy density (Fig. 4e).[26–34] These results demonstrate the satisfying ability of this combination of PC matrix and VO_2 crystal in the storage of Zn^{2+} ion, which suggests that the VO_2-PC would hold promising performance to fulfill the requirements of Zn-based systems for low-grade heat conversion.

The rate performance of VO_2-PC greatly determined by its electrochemical kinetics, which is reasonably studied by CV measurements from 0.2 to 5 mV s^{-1} (Fig. 4f). Typically, the surface-induced capacitance and diffusion-controlled procedure can be indexed according to the relationship between peak current (i) and scan rate (v) as below: $i = av^b$.[35] As known, $b = 0.5$ indicates that the electrochemical process is totally controlled by the diffusion, while $b = 1.0$ represents the capacitance-dominated process. Notably, the calculated b values for peak 1–4 are 0.65, 0.75, 0.88, and 0.83, respectively (Fig. 4g), which reveals that the electrochemical kinetics of VO_2-PC is mainly governed by surface capacitive behavior. Furthermore, the capacity can be detailly divided into capacitance ($k_1 v$) and diffusion-controlled ($k_2 v^{1/2}$) contribution by the following formula:[36]

$$i = i_{cap} + i_{diff} = k_1 v + k_2 v^{1/2} \quad (4)$$

As displayed in Fig. S4f, a high capacitive contribution of 53% can be obtained at the scan rate of 0.2 mV s^{-1}. With the increase of scan rate from 0.2 to 5 mV s^{-1}, the capacitive contribution of VO_2-PC electrode is gradually increased from 53–87.5%, indicating fast charge transfer feature as well as good rate capability. In addition, the galvanostatic intermittent titration technique (GITT) was carried out to investigate the Zn^{2+} diffusion behavior in the VO_2-PC electrode during charging and discharging processes (Fig. 4h). The average diffusion coefficient of Zn^{2+} (D_{Zn}) can be calculated as high as $10^{-10.5}$ cm^2 s^{-1} for the whole charge and discharge, which suggest the fast transport of Zn^{2+} in the cathode. Such high Zn^{2+} diffusion coefficient is corresponded to the continuous porous carbon network and embedded electroactive VO_2. It is worth mentioning that the gradually decrease of D_{Zn} value from about 10^{-10} to 10^{-11} cm^2 s^{-1} in the discharge process can be attributed to the increase of Zn^{2+} content in the VO_2-PC electrode, which further indicates its ability for energy storage.

Energy storage mechanism of ZIBs. Inspired by the superior performances of the VO_2-PC, various *ex-situ* measurements were conducted to reveal the detail reaction mechanism during electrochemical tests. For convenient, the VO_2-PC electrode at specific voltage used for analysis is marked as *state x*, as shown in Fig. 5a. Before the test, the VO_2-PC based ZIB is discharged to 0.2 V and then charged/discharged to

selected voltage state. From the XRD patterns of the VO_2-PC cathode at various states (Fig. 5b), the characteristic peaks at ~ 18º and ~ 25º can be detected in all patterns, which could be assigned to the (100) plane of PTFE (PDF#54-1595) and the (110) plane of monoclinic VO_2 (PDF#81-2392).[37] During the charging process from state I to state III, the interlayer space of (110) plane is gradually reduced because of the slight positive shift of peaks at ~ 25º, which indicates the extraction of electrolyte ions from the VO_2 crystal. Notably, the negative shift of (110) plane during the discharging process further confirm the insertion of electrolyte ions into VO_2, suggesting a highly reversible behavior for ions storage. In addition, the byproduct-free Zn anode is also identified by the corresponding XRD patterns (Fig. 5c), meaning the highly reversible and durable feature. The added peak at ~ 26.3º can be well matched with the (002) plane of graphite, suggesting the successful modification of Zn surface.[35] Moreover, *ex-situ* XPS analyses were employed to explore the chemical states of the initial and the fully charged/discharged electrodes (Fig. 5d-f). In Fig. 5d, the high intensity of Zn 2p peaks in the state V clearly demonstrates the insertion of Zn^{2+} into VO_2. The appearance of the Zn signal at state III is probably caused by the presence of residual zinc salts, indicating that most of Zn^{2+} can be extracted from the VO_2-PC cathode.[18] As known, the GCD processes of V-based ZIBs could be accompanied by the valence change of V element in VO_2 crystals. Compared with the V^{4+} existed in the initial electrode, the V 2p peaks move to low binding energy during discharge together with a high V^{3+}/V^{4+} ratio of 2.65, which suggests the reduction of vanadium-oxide (Fig. 5e). In the charge process, the V^{3+}/V^{4+} ratio decreases to 0.50 and the peaks of Zn 2p are nearly recovered to the initial state due to the oxidization of vanadium. Besides, the content of H_2O gradually enhances during the discharging state and decreases during the charging state, which directly confirms that the solvation effect can promote the diffusion of H_2O to VO_2 along with the insertion of Zn^{2+} (Fig. 5f).[27] The above results propose that the VO_2-PC based ZIBs exhibit a hybrid energy storage mechanism including the ions adsorption on PC and the Zn^{2+} reaction in VO_2.

Performance of wearable ZTGCs. Inspired by the satisfying performance of ZTGCs for energy storage and conversion, we further designed a quasi-solid-state device using polyacrylamide (PAM) based gel for wearable application (Fig. 6a). Considering that the Zn^{2+} can extract from hot part and the react with $Zn_xVO_2{\cdot}yH_2O$ and Zn electrodes, the VO_2 cathode acts as electrode for both energy conversion and storage. In such wearable ZTGCs, the Zn^{2+} also can diffuse to VO_2 and react into $Zn_xVO_2{\cdot}yH_2O$ after fully discharged procedure. As profiled in Fig. 6b, the ZTGC can charge and discharge under multiple modes. When the ZTGC is thermally charged using temperature difference between skin temperature (T_{skin}) and ambient temperature ($T_{ambient}$), the output voltage can slowly reach to ~ 0.6 V (Fig. 6b). It is worth mentioning that almost 1.3 V can be obtained with two ZTGCs in series (ΔT of ~ 12 K). Such integrated devices can be galvanostatically charged from thermal charge state (~ 1.3 V) to fully charged state (3.2 V). To demonstrate the practical application of such ZTGCs in real conditions via a facile way, only two pouch ZTGCs were connected in series to power a smart watch (Fig. 6c-e), which is much easier than that of practical e-TEs or i-TEs integration. Moreover, as-constructed ZTGCs can work normally even under harsh conditions (Fig. 6e), confirming the availability and durability of developed ZTGCs.

Discussion

In summary, we have demonstrated the design and construction of ZTGCs with Zn anode and VO_2-PC hybrid cathode, which is prepared by a universal metal coordination strategy, for high-performance Zn^{2+} storage and low-grade heat conversion. It is worth mentioning that the evenly distributed VO_2 in the porous carbon provides abundant electroactive sites, delivering high storage capability and fast kinetics of Zn^{2+}. The carbon matrix acts as continuous pathways for charge transport and channels for electrolyte ions diffusion. Consequently, a high Seebeck coefficient of 8-69.2 mV K^{-1} can be achieved by the change of temperature difference, which is beneficial to the synergistical combination of the thermogalvanic effect and diffusion process. As a proof-of-concept, only one ZGTCs exhibits a high output voltage of ~ 1 V, and a record-breaking output power of 1220 μW under the temperature difference of 45 K. Moreover, the VO_2-PC exhibits an excellent Zn-ion storage behavior, such as a high specific capacity (588 mAh g^{-1} at 0.1 A g^{-1}), good rate capability (80 mAh g^{-1} even at 20 A g^{-1}), and an impressive cycling stability over 50000 cycles. Moreover, two quasi-solid-state ZTGCs in series show high availability and durability in the electronics area. All the findings have confirmed that the proposed ZTGC would be a potential candidate for promising energy storage and conversion, and the detailed studies of involved mechanisms may provide a deep insight for the development of zinc-based devices.

Methods

Preparation of VO_2-PC. Typically, 1.0 g of ammonium metavanadate and 0.25 g dopamine hydrochloride were dissolved in 100 mL deionized water. Then, 200 mL of ethanol was added into above solution with stirring for about 10 min. After that, 1.5 mL of $NH_3 \cdot H_2O$ was dropped into it and stirring for another 2 h to obtain vanadium-polydopamine (V-PDA) precursors. Finally, the VO_2-PC was prepared by the pyrolysis of V-PDA at 500 ºC for 3 h with a heating rate of 3 ºC min^{-1} under argon flow. In addition, the Mo_4O_8-PC and W_3O_9-PC were synthesized by the same strategy as above, only changing the added metal source to ammonium molybdate tetrahydrate and ammonium metatungstate.

Electrochemical measurements. All the electrochmical performances for the conversion of low-grade heat to electricity were evaluated on a standard electrochemical workstation (CHI 660C) with a non-isothermal H cell using 0.5 mol L^{-1} $Zn(CF_3SO_3)_2$. Typically, the working electrode was prepared by the coating of as-obtained samples onto graphite paper together with acetylene and polyvinylidene fluoride according to a mass ratio of 7:2:1. It is worth mentioning that the mass loading in working electrode was about 1.2 mg cm^{-2}. Besides, the Zn anode used was modified by graphite following our previous work.[35] For ZIBs tests, the CV curves and GITT were performed by the Biologic VMP-300 workstation. The GCD measurements and cycling stability were collected on the CT3001A Land Battery Test System. Notably, the specific capacity and energy density of ZIBs were recorded directly from Land Battery Test System.

The quasi-solid-state ZTGCs were constructed by sandwiching the Zn-G anode, gel electrolyte and VO_2-PC cathode. The gel electrolyte was prepared through a polymerization of acrylamide (AM) and subsequent

electrolyte immersion. Briefly, 2.5 g of AM, 1.5 mg of *N*,*N*'-methylenebisacrylamide, and 10 μL of *N*,*N*,*N*',*N*'-tetramethylethylenediamine were added into 10 mL of deionized water part by part with vigorous stirring at ~ 0 ºC. After that, 0.25 g of potassium persulfate were dispersed into above solution. When polymerizing with a UV lamp (60 W) for about 20 min, a transparent hydrogel was prepared. Finally, such hydrogel was immersed in electrolyte solution to fabricate flexible $Zn(CF_3SO_3)_2$-PAM gel electrolyte.

Material characterizations. Scanning electron microscope (SEM) and transmission electron microscope (TEM) were employed on Hitachi S-4800 and JEOL JEM-2100, respectively. Powder X-ray diffraction (XRD) was obtained by a PANalytical Empyrean diffractometer with Cu Kα radiation (λ = 1.5406 Å). X-ray photoelectron spectrometer (XPS) was carried out by the KRATOS AXIS SUPRA instrument. Raman spectroscopy was conducted by the Horiba Scientific LabRAM HR.

Declarations

Acknowledgments

This work was supported by the National Natural Science Foundation of China (U1802256, 21773118, 21875107), Leading Edge Technology of Jiangsu Province (BK20202008), Key Research and Development Program in Jiangsu Province (BE2018122), Postgraduate Research & Practice Innovation Program of Jiangsu Province (KYCX21_0204) and Priority Academic Program Development of Jiangsu Higher Education Institutions (PAPD).

Author contributions

Z. L. carried out the experiment. Z. L., Y. X. and Y. A. designed and evaluated the electrochemical performances. L. W. analyzed the structural characterization and electrochemical results. Z. L., Y. S. and T. M. organized the figures. H. D. Y. X. and X. Z. supervised the whole work. All authors co-discussed the results and wrote the manuscript.

Competing interests

The authors declare no competing interests.

Additional information

Supplementary information is available for this paper at

Correspondence and requests for materials should be addressed to X.Z.

References

1. He, J. & Tritt, T. M. Advances in thermoelectric materials research: Looking back and moving forward. *Science* **357**, eaak9997 (2017).

2. Han, C. G., Qian, X., Li, Q., Deng, B., Zhu, Y., Han, Z., Zhang, W., Wang, W., Feng, S.P., Chen, G. & Liu, W. Giant thermopower of ionic gelatin near room temperature. *Science* **368**, 1091-1098 (2020).

3. Wang, H. & Yu, C. Organic thermoelectrics: Materials preparation, performance optimization, and device integration. *Joule* **3**, 53-80 (2019).

4. Tan, G., Zhao, L.-D. & Kanatzidis, M. G. Rationally designing high-performance bulk thermoelectric materials. *Chem. Rev*. **116**, 12123-12149 (2016).

5. Wang, X., Huang, Y. T., Liu, C., Mu, K., Li, K. H., Wang, S., Yang, Y., Wang, L., Su, C. H. & Feng, S. P. Direct thermal charging cell for converting low-grade heat to electricity. *Nat. Commun*. **10**, 4151 (2019).

6. Chen, D., Li, Z., Jiang, J., Wu, J., Shu, N. & Zhang, X. Influence of electrolyte ions on rechargeable supercapacitor for high value-added conversion of low-grade waste heat. *J. Power Sources* **465**, 228263 (2020).

7. Kim, B., Hwang, J. U. & Kim, E. Chloride transport in conductive polymer films for an n-type thermoelectric platform. *Energy Environ. Sci*. **13**, 859-867 (2020).

8. Yang, P., Liu, K., Chen, Q., Mo, X., Zhou, Y., Li, S., Feng, G. & Zhou, J. Wearable thermocells based on gel electrolytes for the utilization of body heat. *Angew. Chem. Int. Ed*. **55**, 12050-12053 (2016).

9. Yu, B., Duan, J., Cong, H., Xie, W., Liu, R., Zhuang, X., Wang, H., Qi, B., Xu, M., Wang, Z. L. & Zhou, J. Thermosensitive crystallization–boosted liquid thermocells for low-grade heat harvesting. *Science* **370**, 342-346 (2020).

10. Poletayev, A. D., McKay, I. S., Chueh, W. C. & Majumdar, A. Continuous electrochemical heat engines. *Energy Environ. Sci*. **11**, 2964-2971 (2018).

11. Blanc, L. E., Kundu, D. & Nazar, L.F. Scientific challenges for the implementation of Zn-ion batteries. *Joule* **4**, 771-799 (2020).

12. Zhang, N., Chen, X., Yu, M., Niu, Z., Cheng, F. & Chen, J. Materials chemistry for rechargeable zinc-ion batteries. *Chem. Soc. Rev.* **49**, 4203-4219 (2020).

13. Jia, X., Liu, C., Neale, Z. G., Yang, J. & Cao, G. Active materials for aqueous zinc ion batteries: Synthesis, crystal structure, morphology, and electrochemistry. *Chem. Rev*. **120**, 7795-7866 (2020).

14. Zhang, Y., Wan, F., Huang, S., Wang, S., Niu, Z. & Chen, J. A chemically self-charging aqueous zinc-ion battery. *Nat. Commun*. **11**, 2199 (2020).

15. Meng, Y., Liu, P., Zhou, W., Ding, J. & Liu, J. Bioorthogonal DNA adsorption on polydopamine nanoparticles mediated by metal coordination for highly robust sensing in serum and living cells. *ACS Nano* **12**, 9070-9080 (2018).

16. Li, Z., Ren, Y., Mo, L., Liu, C., Hsu, K., Ding, Y., Zhang, X., Li, X., Hu, L. & Ji, D. Impacts of oxygen vacancies on zinc ion intercalation in VO_2. *ACS Nano* **14**, 5581-5589 (2020).

17. Li, R. & Liu, C.-Y. VO_2 (B) nanospheres: Hydrothermal synthesis and electrochemical properties. *Mater. Res. Bull.* **45**, 688-692 (2010).

18. Chen, L., Ruan, Y., Zhang, G., Wei, Q., Jiang, Y., Xiong, T., He, P., Yang, W., Yan, M., An, Q. & Mai, L. Ultrastable and high-performance Zn/VO_2 battery based on a reversible single-phase reaction. *Chem. Mater.* **31**, 699-706 (2019).

19. Luo, H., Wang, B., Wang, C., Wu, F., Jin, F., Cong, B., Ning, Y., Zhou, Y., Wang, D. & Liu, H. Synergistic deficiency and heterojunction engineering boosted VO_2 redox kinetics for aqueous zinc-ion batteries with superior comprehensive performance. *Energy Storage Mater.* **33**, 390-398 (2020).

20. Wang, H., Zhu, Y., Kim, S. C., Pei, A., Li, Y., Boyle, D. T., Wang, H., Zhang, Z., Ye, Y. & Huang, W. Underpotential lithium plating on graphite anodes caused by temperature heterogeneity. *P. Natl. Acad. Sci.* **117**, 29453-29461 (2020).

21. Duan, J., Yu, B., Liu, K., Li, J., Yang, P., Xie, W., Xue, G., Liu, R., Wang, H. & Zhou, J. PN conversion in thermogalvanic cells induced by thermo-sensitive nanogels for body heat harvesting. *Nano Energy* **57**, 473-479 (2019).

22. Kim, S. J., We, J. H. & Cho, B. J. A wearable thermoelectric generator fabricated on a glass fabric. *Energy Environ. Sci.* **7**, 1959-1965 (2014).

23. Oh, J. Y., Lee, J. H., Han, S. W., Chae, S. S., Bae, E. J., Kang, Y. H., Choi, W. J., Cho, S. Y., Lee, J.-O. & Baik, H. K. Chemically exfoliated transition metal dichalcogenide nanosheet-based wearable thermoelectric generators. *Energy Environ. Sci.* **9**, 1696-1705 (2016).

24. Kim, C. S., Lee, G. S., Choi, H., Kim, Y. J., Yang, H. M., Lim, S. H., Lee, S.-G. & Cho, B. J. Structural design of a flexible thermoelectric power generator for wearable applications. *Applied Energy* **214**, 131-138 (2018).

25. Ding, J., Du, Z., Gu, L., Li, B., Wang, L., Wang, S., Gong, Y. & Yang, S. Ultrafast Zn^{2+} intercalation and deintercalation in vanadium dioxide. *Adv. Mater.* **30**, 1800762 (2018).

26. Ding, J., Du, Z., Li, B., Wang, L., Wang, S., Gong, Y. & Yang, S. Unlocking the potential of disordered rocksalts for aqueous zinc-ion batteries. *Adv. Mater.* **31**, 1904369 (2019).

27. Chen, L., Yang, Z. & Huang, Y. Monoclinic VO_2(D) hollow nanospheres with super-long cycle life for aqueous zinc ion batteries. *Nanoscale* **11**, 13032-13039 (2019)..

28. Zhao, J., Ren, H., Liang, Q., Yuan, D., Xi, S., Wu, C., Manalastas, W., Ma, J., Fang, W., Zheng, Y., et al. High-performance flexible quasi-solid-state zinc-ion batteries with layer-expanded vanadium oxide cathode and zinc/stainless steel mesh composite anode. *Nano Energy* **62**, 94-102 (2019)..

29. Liu, Y.-Y., Lv, T.-T., Wang, H., Guo, X.-T., Liu, C.-S. & Pang, H. Nsutite-type VO_2 microcrystals as highly durable cathode materials for aqueous zinc-ion batteries. *Chem. Eng. J.* **417**, 128408 (2021).

30. Deka Boruah, B., Mathieson, A., Park, S.K., Zhang, X., Wen, B., Tan, L., Boies, A. & De Volder, M. Vanadium dioxide cathodes for high-rate photo-rechargeable zinc-ion batteries. *Adv. Energy Mater.* **11**, 2100115 (2021).

31. Luo, H., Wang, B., Wu, F., Jian, J., Yang, K., Jin, F., Cong, B., Ning, Y., Zhou, Y., Wang, D., et al. Synergistic nanostructure and heterointerface design propelled ultra-efficient in-situ self-transformation of zinc-ion battery cathodes with favorable kinetics. *Nano Energy* **81**, 105601 (2021).

32. Wang, L., Huang, K.-W., Chen, J. & Zheng, J. Ultralong cycle stability of aqueous zinc-ion batteries with zinc vanadium oxide cathodes. *Sci. Adv.* **5**, eaax4279 (2019).

33. Liu, C., Neale, Z., Zheng, J., Jia, X., Huang, J., Yan, M., Tian, M., Wang, M., Yang, J. & Cao, G. Expanded hydrated vanadate for high-performance aqueous zinc-ion batteries. *Energy Environ. Sci.* **12**, 2273-2285 (2019).

34. Liao, M., Wang, J., Ye, L., Sun, H., Wen, Y., Wang, C., Sun, X., Wang, B. & Peng, H. A deep-cycle aqueous zinc-ion battery containingan oxygen-deficient vanadium oxide cathode. *Angew. Chem. Int. Ed.* **132**, 2293-2298 (2020).

35. Li, Z., Wu, L., Dong, S., Xu, T., Li, S., An, Y., Jiang, J. & Zhang, X. Pencil drawing stable interface for reversible and durable aqueous zinc-ion batteries. *Adv. Funct. Mater* **31**, 2006495 (2020).

36. Li, Z., Chen, D., An, Y., Chen, C., Wu, L., Chen, Z., Sun, Y. & Zhang, X. Flexible and anti-freezing quasi-solid-state zinc ion hybrid supercapacitors based on pencil shavings derived porous carbon. *Energy Storage Mater.* **28**, 307-314 (2020).

37. Huang, J., Wang, Z., Hou, M., Dong, X., Liu, Y., Wang, Y. & Xia, Y. Polyaniline-intercalated manganese dioxide nanolayers as a high-performance cathode material for an aqueous zinc-ion battery. *Nat. Commun.* **9**, 1-8 (2018).

Figures

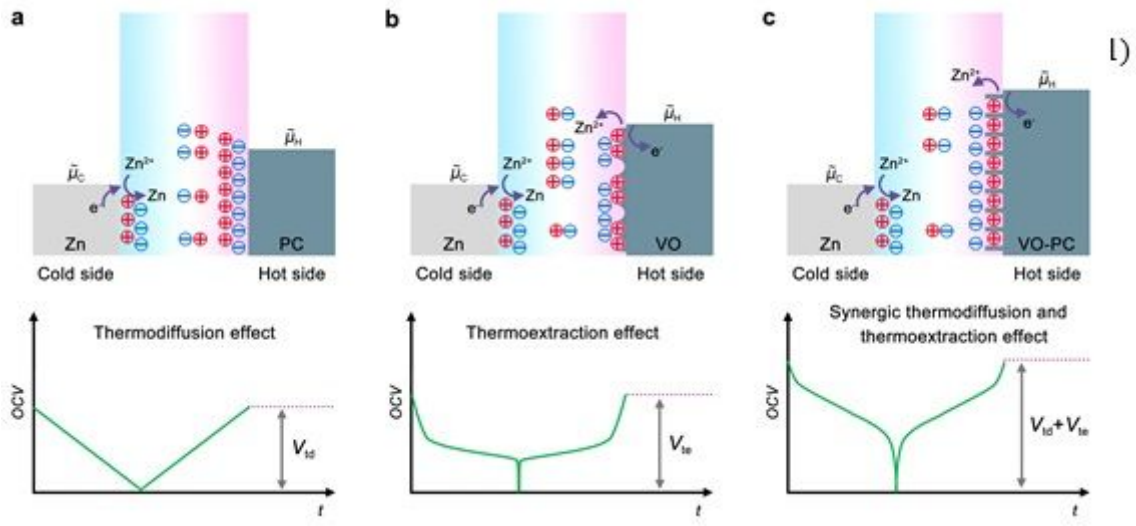

Figure 1

Concept and working mechanism of Zn-based thermally chargeable systems. a Thermodiffusion effect, b thermoextraction effect and c synergistic effect.

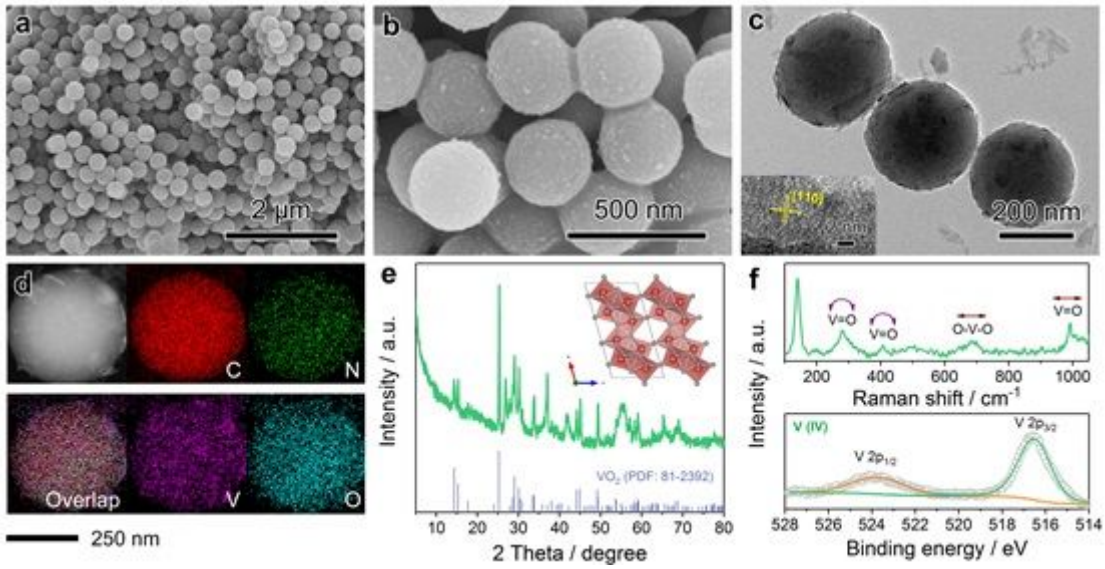

Figure 2

Morphology and structural characterization of the VO2-PC. a,b SEM and c TEM images. d EDX mapping images. e XRD pattern and the crystal structure of the VO2-PC. f Raman spectrum and high-resolution XPS spectrum of V 2p.

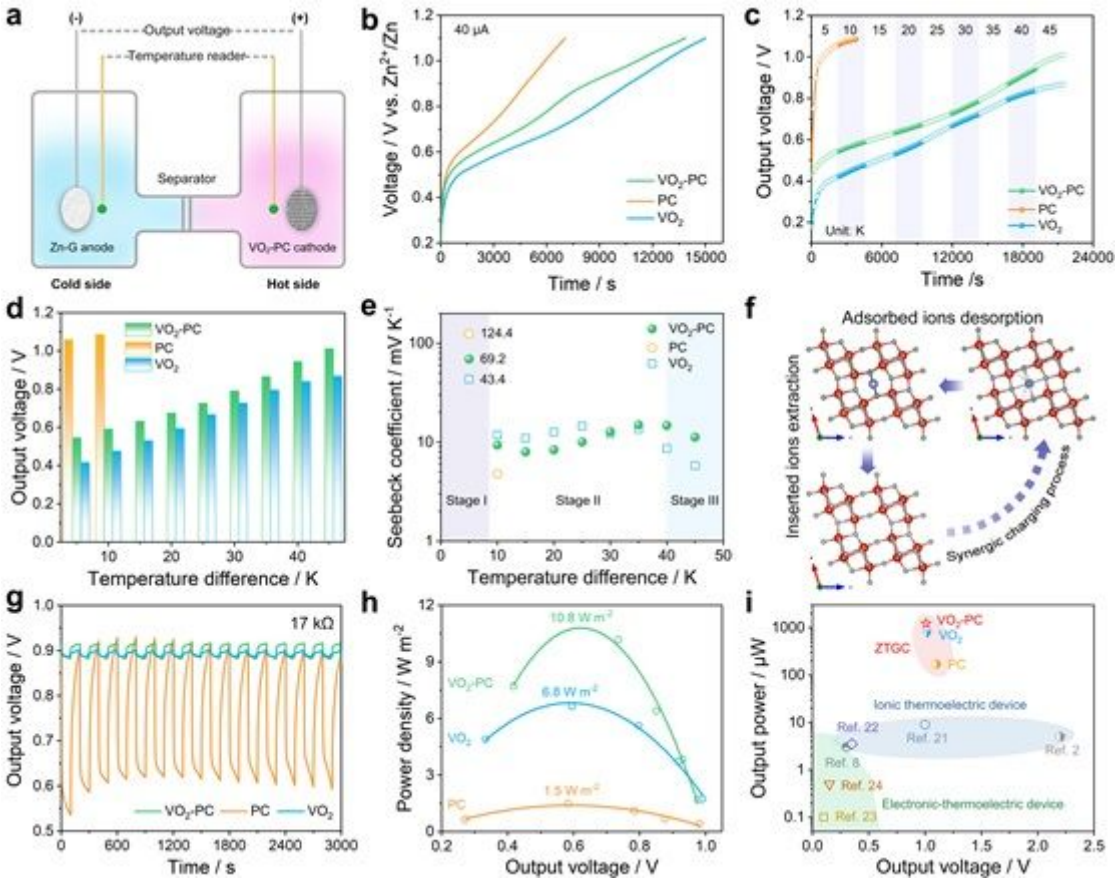

Figure 3

Construction and performance of ZTGCs. a The schematic diagram of non-isothermal cell. b Electrochemical charge curves with a current of 40 μA. c Evolution of the output voltage with various temperature gradients. d The output voltage and e Seebeck coefficient obtained at various temperature differences. f The corresponding structural changes of VO2 during energy conversion. g The discharging curves with a load of 17 kΩ. h Plots of current densities and power densities under various output voltages. i Comparison in output power and voltage.

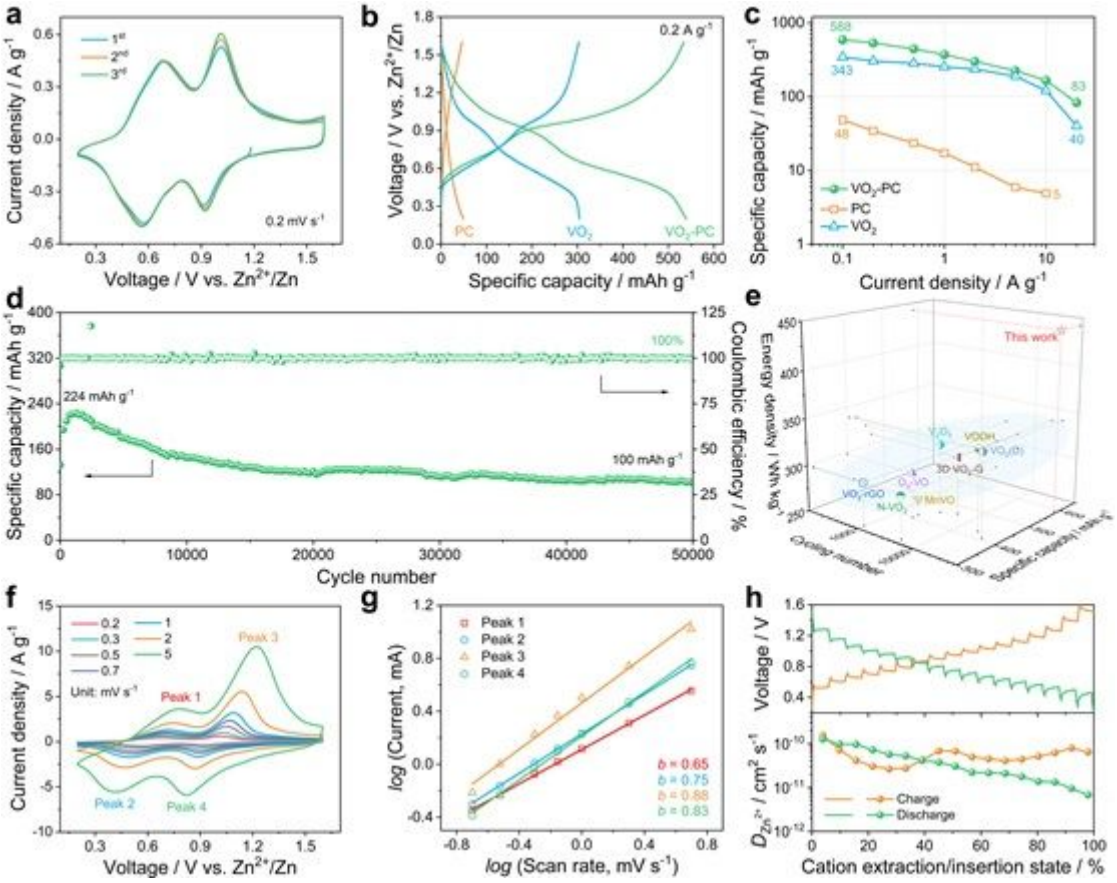

Figure 4

Electrochemical performance of ZIBs with various electrodes. a CV curves for the initial 3 cycles of VO2-PC at 0.2 mV s−1. b GCD curves, c Ragone plots, and d cycling stability at 10 A g−1. e Comparison of main electrochemical parameters of the VO2-PC based ZIB with other reported devices. f CV curves at various scan rates. g The corresponding log (current) vs. log (scan rate) of each redox peak. h GITT curves and Zn2+ diffusion coefficient at charging/discharging.

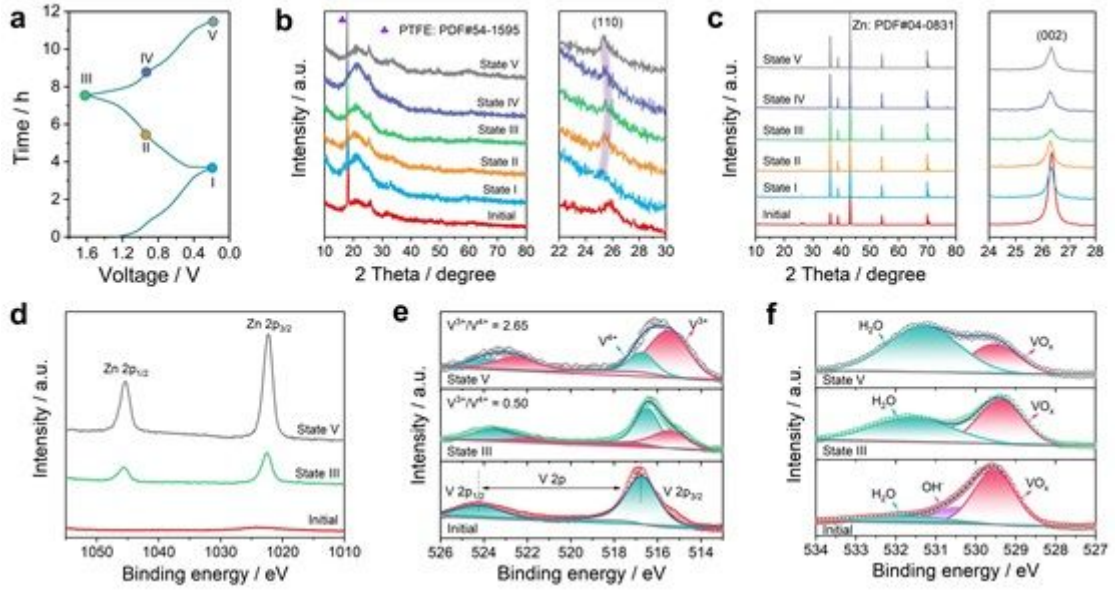

Figure 5

The mechanism of VO2-PC based ZIBs. a The GCD curves at 0.1 A g−1. b,c The corresponding ex-situ XRD patterns of b VO2-PC cathode and c Zn-G anode. d-f The corresponding ex-situ XPS spectra of d Zn 2p, e V 2p, and f O 1s.

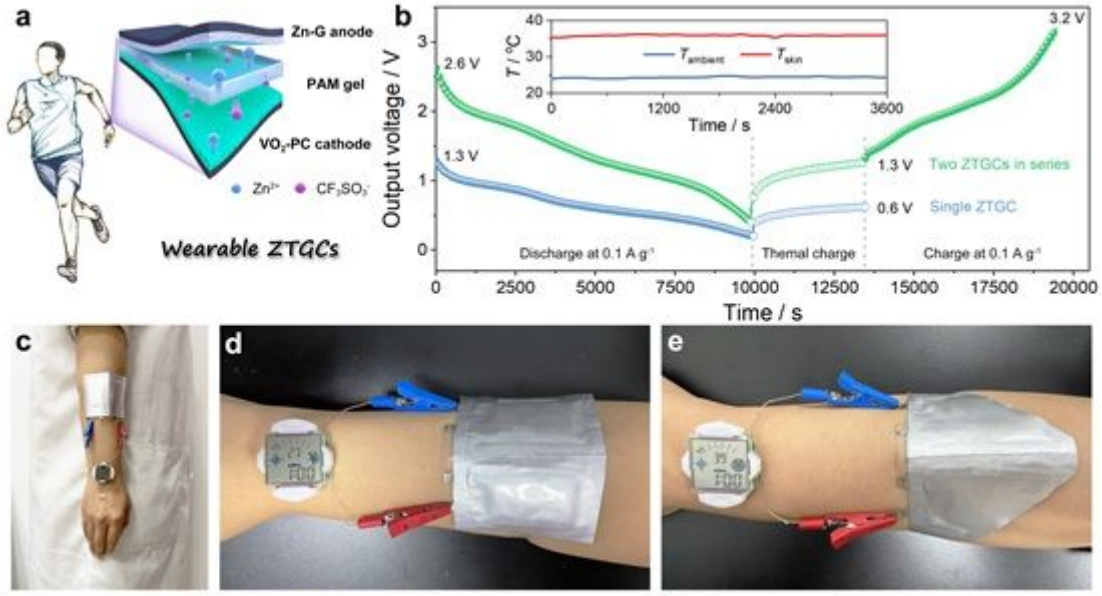

Figure 6

Proof-of-concept of ZTGCs at various modes. a Schematic drawing of the wearable ZTGCs. b charge/discharge process at galvanostatic and/or thermal models. The inset showed the change of body heat and ambient temperature. c-e a smart watch powered by two ZTGCs in series at c,d initial state and e the harsh condition.

Supplementary Files

This is a list of supplementary files associated with this preprint. Click to download.

- SupportingInformation.docx
- GraphicalAbstract.jpg